# Baroclinic and Barotropic Annular Variability in the Northern Hemisphere

DAVID W. J. THOMPSON AND YING LI

*Department of Atmospheric Science, Colorado State University, Fort Collins, Colorado*

(Manuscript received 14 April 2014, in final form 28 August 2014)

ABSTRACT

Large-scale variability in the Northern Hemisphere (NH) circulation can be viewed in the context of three primary types of structures: 1) teleconnection patterns, 2) a barotropic annular mode, and 3) a baroclinic annular mode. The barotropic annular mode corresponds to the northern annular mode (NAM) and has been examined extensively in previous research. Here the authors examine the spatial structure and time-dependent behavior of the NH baroclinic annular mode (NBAM).

The NAM and NBAM have very different signatures in large-scale NH climate variability. The NAM emerges as the leading principal component (PC) time series of the *zonal-mean* kinetic energy. It dominates the variance in the wave fluxes of momentum, projects weakly onto the eddy kinetic energy and wave fluxes of heat, and can be modeled as Gaussian red noise with a time scale of ~10 days. In contrast, the NBAM emerges as the leading PC time series of the *eddy* kinetic energy. It is most clearly identified when the planetary-scale waves are filtered from the data, dominates the variance in the synoptic-scale eddy kinetic energy and wave fluxes of heat, and has a relatively weak signature in the zonal-mean kinetic energy and the wave fluxes of momentum. The NBAM is marked by weak but significant enhanced spectral power on time scales of ~20–25 days.

The NBAM is remarkably similar to its Southern Hemisphere counterpart despite the pronounced interhemispheric differences in orography and land–sea contrasts.

## 1. Introduction

Large-scale variability in the extratropical circulation is often examined in the context of two primary classes of structures: teleconnection patterns and annular modes.

Teleconnection patterns are typically defined on the basis of significant negative correlations between widely separated points in the geopotential height field (e.g., Wallace and Gutzler 1981). They are generally regional in scale and thus project most strongly onto climate variability over specific sectors of the hemisphere. In contrast, the northern and southern annular modes (the NAM and SAM, respectively) are typically defined as the leading empirical orthogonal functions of the hemispheric-scale geopotential height and/or zonal wind fields (e.g., Kidson 1988; Hartmann and Lo 1998; Thompson and Wallace 2000). In contrast to most teleconnection patterns, they are hemispheric in scale and thus project onto climate variability throughout the extratropics of their respective hemispheres.

Teleconnection patterns are frequently viewed in the context of their zonally *asymmetric* components. The Pacific–North America pattern is dominated by wavelike anomalies in the geopotential height field that stretch along a great circle route from the central North Pacific to eastern North America (Wallace and Gutzler 1981; Quadrelli and Wallace 2004); the North Atlantic Oscillation is characterized by north–south fluctuations in the geopotential height field that have the largest amplitude in the North Atlantic sector (e.g., Wallace and Gutzler 1981; Hurrell 1995). In contrast, the NAM and SAM are commonly viewed in the context of their zonally *symmetric* components. Both are characterized by barotropic fluctuations in the extratropical circulation that exhibit a high degree of longitudinal symmetry. The North Atlantic Oscillation teleconnection pattern also has a pronounced zonally symmetric component and may be viewed as a regional expression of the NAM (Wallace 2000).

In recent work (Thompson and Woodworth 2014, hereafter TW), we have argued that large-scale variability in the Southern Hemisphere (SH) extratropical flow can be examined in the context of a third type of

*Corresponding author address:* David W. J. Thompson, Dept. of Atmospheric Science, Colorado State University, Campus Delivery 1782, Ft. Collins, CO 80523.
E-mail: davet@atmos.colostate.edu

DOI: 10.1175/JAS-D-14-0104.1

structure: a *baroclinic* annular mode. The key results of TW are the following:

1) The SAM is the leading pattern of variability in the SH *zonal-mean kinetic energy*, and it may be viewed as a *barotropic* annular mode. It explains large fractions of the variance in the wave fluxes of momentum, but has a very weak projection onto the eddy fluxes of heat and the eddy kinetic energy.
2) In contrast, the leading pattern of variability in the SH *eddy kinetic energy* may be viewed as a *baroclinic* annular mode. Like the SAM, the southern baroclinic annular mode has a distinct zonally symmetric component. But unlike the SAM, it projects strongly onto the eddy fluxes of heat, and only weakly onto the zonal-mean kinetic energy and eddy fluxes of momentum.
3) The SAM and its baroclinic counterpart play very different roles in SH climate variability. They have contrasting roles in the extratropical energy cycle. They have very different projections on surface climate. And notably, they have very different signatures in the frequency domain: the SAM can be modeled as Gaussian red noise with a time scale of ~10 days (Hartmann and Lo 1998; Lorenz and Hartmann 2001); the southern baroclinic annular mode exhibits marked variability on ~20–30-day time scales (TW; Thompson and Barnes 2014).

The purpose of this paper is to extend the analyses of TW to the Northern Hemisphere (NH). We will demonstrate that the NH circulation exhibits a baroclinic annular mode that is very similar to its SH counterpart despite the notable interhemispheric differences in orography and land–sea contrasts. In section 3, we develop a procedure for identifying baroclinic annular variability in the NH. In section 4, we investigate the signature of the NH baroclinic annular mode in the zonal-mean circulation, and contrast it to the NH barotropic annular mode (the NAM). In section 5, we examine the longitudinally varying structure of the NH baroclinic annular mode and examine the teleconnectivity between eddy activity in the North Atlantic and North Pacific storm-track regions. In section 6, we examine the spectral characteristics of the NH baroclinic annular mode. Conclusions are provided in section 7.

## 2. Data and methods

All analyses are based on the Interim European Centre for Medium-Range Weather Forecasts Re-Analysis dataset (ERA-Interim; Dee et al. 2011). The reanalyses output are available on a 1.25° × 1.25° mesh and at four-times-daily resolution. The results are based on daily-mean versions of the data for the period 1979–2011. Daily mean precipitation is calculated by averaging total precipitation at 0000 and 1200 UTC at forecast steps of 6 and 12 h. Anomalies are formed by subtracting the long-term mean seasonal cycle from the data at all time steps.

Throughout the study, brackets denote zonal-mean quantities and asterisks denote departures from the zonal mean. The zonal-mean eddy kinetic energy is defined as $\frac{1}{2}[u^{*2} + v^{*2}]$, the zonal-mean eddy fluxes of momentum are defined as $[u^*v^*]$, and the zonal-mean eddy fluxes of heat are defined as $[v^*T^*]$. Eddy fluxes are calculated at four-times-daily resolution and averaged to form daily-mean versions of the fluxes.

In cases where we use empirical orthogonal function–principal component (EOF–PC) analyses, the data are weighted by the square root of the cosine of latitude and the mass represented by each vertical level in the ERA-Interim before calculating the covariance matrix of the data.

As discussed in section 3, the wind data used to identify baroclinic annular variability are spatially filtered to remove the contributions of planetary-scale eddies to the eddy kinetic energy. Planetary-scale eddies are defined here as variations on spatial scales of zonal wavenumbers 1–3; synoptic-scale eddies are defined as variations on spatial scales of zonal wavenumbers 4 and higher.

Power spectra for time series that span all calendar days are found by 1) calculating the spectra for subsets of the time series that are 500 days in length with 250-days' overlap between adjacent subsets (split-cosine-bell tapering is applied to 5% of the data on each end of the subset time series); 2) averaging the power spectra over all subsets of the time series; and 3) applying a three-point running mean to the resulting mean power spectrum. Power spectra for time series limited to the warm and cold seasons are based on subsets that are 183 days in length for the warm season (April–September) and 182 days in length for the cold season (October–March) with no overlap between subsets.

The statistical significance of the correlation coefficient is assessed using the $t$ statistic. The confidence levels on the power spectrum are estimated from the chi-squared distribution and a red-noise fit to the spectrum. As discussed in the appendix, the lag-1 autocorrelations used to estimate the red-noise fits are calculated from high-pass-filtered versions of the time series. In the case of correlations, the effective number of degrees of freedom ($N^*$) are estimated as

$$N^* = N\frac{1 - r_1 r_2}{1 + r_1 r_2}, \qquad (1)$$

where $N$ is the number of time steps used in the correlations, and $r_1$ and $r_2$ are the lag-1 autocorrelations of the time series being correlated (Bretherton et al. 1999). In the case of power spectra, the degrees of freedom are estimated as the ratio of 1) the number of time steps in the time series to 2) the number of independent spectral estimates in the power spectrum. Additional details on the significance tests and red-noise fits to the data are provided as necessary in the results sections.

## 3. Defining baroclinic annular variability in the Northern Hemisphere

In this section, we develop an index for characterizing baroclinic annular variability in the NH. Throughout the study, the southern and northern *barotropic* annular modes are denoted as the SAM and NAM, respectively, whereas the southern and northern *baroclinic* annular modes are denoted as the SBAM and NBAM, respectively.

The left column in Fig. 1 reviews the latitude–lag structure of the southern baroclinic annular mode (the SBAM) in two key fields: the zonal-mean eddy fluxes of heat at 850 hPa and the eddy kinetic energy at 300 hPa. As in TW, the SBAM is defined as the leading PC time series of the zonal-mean eddy kinetic energy for all levels and latitudes within the domain 1000–200 hPa and 20°–70°S. By definition, the "positive polarity" of the SBAM is defined as periods when the hemispheric-mean eddy kinetic energy is anomalously positive, and vice versa. All results in Fig. 1 are based on daily-mean data for all calendar months.

Figure 1a shows the unfiltered, zonal-mean fields of the eddy fluxes of heat at 850 hPa (shading) and the eddy kinetic energy at 300 hPa (contours) regressed onto the SBAM index as a function of lag and latitude. The figure is identical to Fig. 3b from TW, but is calculated using a slightly different time period. As noted in that study, the positive polarity of the SBAM is associated with poleward eddy heat flux anomalies and positive eddy kinetic energy anomalies that span much of the SH middle latitudes. The heat flux anomalies precede the eddy kinetic energy anomalies by ~1–2 days, consistent with the time lag between the generation of wave activity in the lower troposphere and the generation of eddy kinetic energy aloft (Simmons and Hoskins 1978).

Figures 1c and 1e show the contributions of the synoptic- and planetary-scale waves to the regressions in the top panel (synoptic- and planetary-scale waves are defined in section 2). As evidenced in the left column of Fig. 1, variations in the SBAM are associated almost entirely with eddies on synoptic spatial scales. The dominant role of synoptic-scale eddies in association with the SBAM is consistent with 1) the relatively weak amplitudes of planetary-scale waves in the SH and 2) the notion that the SBAM owes its existence to two-way feedbacks between the baroclinicity and the eddy fluxes of heat by synoptic-scale waves (Thompson and Barnes 2014).

The right column in Fig. 1 shows analogous results calculated for the NH. In all three panels, the regressions are based on the leading PC time series of the zonal-mean eddy kinetic energy for all levels and latitudes within the domain 1000–200 hPa and 20°–70°N. As in the SH, the leading PC of NH eddy kinetic energy is marked by same sign fluctuations in both the eddy kinetic energy and eddy fluxes of heat that span much of the midlatitudes (Fig. 1b). However, unlike the SH, the anomalies have a relatively complicated spatial structure, and derive in roughly equal parts from synoptic- and planetary-scale eddies (Figs. 1d,f). Hence, the leading pattern of variability in the NH eddy kinetic energy field includes a notable contribution from the planetary-scale eddies that is not reflected in association with the SBAM.

To the extent that baroclinic annular variability reflects the dynamics of baroclinic waves, it follows that a physically meaningful index of baroclinic annular variability should isolate the variance in the eddy kinetic field associated with synoptic-scale eddies. Filtering the eddy kinetic energy field to isolate the variance associated with synoptic-scale eddies is not necessary in the SH, where the planetary-scale waves have relatively weak amplitude. But as evidenced in Fig. 1, it is essential in the NH, where the planetary-scale waves make a prominent contribution to the leading EOF of the eddy kinetic energy. For this reason, we will define the time series of the northern baroclinic annular mode (the NBAM) as the leading PC time series of the eddy kinetic energy associated with wavenumbers 4 and higher. As done for the SH, the PC time series is calculated for all levels and latitudes within the domain 1000–200 hPa and 20°–70°N. The patterns associated with the resulting NBAM index are explored in the following sections.

## 4. Structure of the NAM and NBAM in the zonal-mean circulation

Figures 2–5 compare the structures of the NAM and NBAM in the extratropical zonal-mean circulation. The NAM index is defined as the leading PC time series of the anomalous daily-mean, zonal-mean zonal wind for all levels and latitudes in the domain 1000–200 hPa and 20°–70°N. The resulting index is very similar to that used in other studies; for example, the correlation coefficient between monthly-mean values of the NAM index used here and the leading PC time series of the monthly-mean

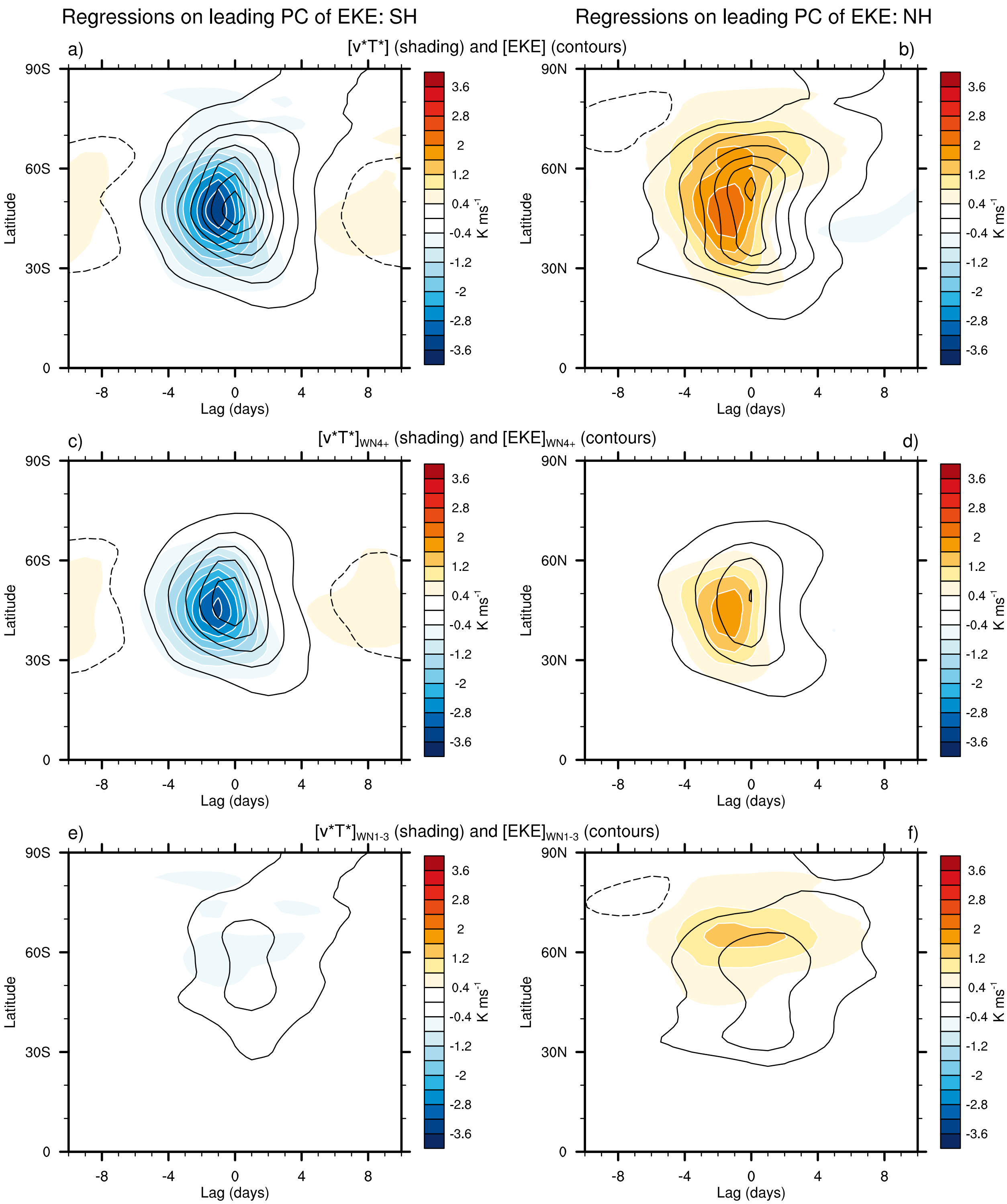


FIG. 1. Latitude–lag structure of the leading PCs of eddy kinetic energy (EKE) in the (a),(c),(e) Southern Hemisphere (SH) and (b),(d),(f) Northern Hemisphere (NH). Results are based on daily-mean data for all calendar months. (top) Daily-mean, zonal-mean values of the eddy fluxes of heat at 850 hPa (shading) and EKE at 300 hPa (contours) regressed onto the leading PC time series of EKE. The PC time series are derived from analysis of unfiltered EKE within 1000–200 hPa and 20°–70°. (middle),(bottom) Components of the regressions in (top) that derive from (middle) synoptic- (zonal wavenumbers ≥ 4) and (bottom) planetary-scale (zonal wavenumbers 1–3) waves; shading and contours as in (top). Negative lags denote the field leads the PC time series and vice versa. Contours are at −3.5, 3.5, 10.5 $m^2 s^{-2}$, etc.

TABLE 1. Variances explained by the PCs considered in this study. The PCs are calculated for zonal-mean, daily-mean data between 1000–200 hPa and 20°–70°N for the fields indicated. ZKE denotes the zonal-mean kinetic energy; $EKE_{WN4+}$ denotes the zonal-mean eddy kinetic energy associated with zonal wavenumbers ≥ 4; Atlantic and Pacific denote data restricted to longitude bands 90°W–50°E and 110°E–110°W, respectively; cold and warm denote data restricted to October–March and April–September, respectively. All leading PCs are well separated from the second PC as per the criterion outlined in North et al. (1982).

| | *U* (NAM) | ZKE | $EKE_{WN4+}$ (NBAM) | $EKE_{WN4+}$ (Atlantic) | $EKE_{WN4+}$ (Pacific) | $EKE_{WN4+}$ (Cold) | $EKE_{WN4+}$ (Warm) |
|---|---|---|---|---|---|---|---|
| PC 1 | 34.1 | 37.0 | 43.0 | 42.2 | 47.5 | 45.4 | 40.9 |
| PC 2 | 25.4 | 27.1 | 18.3 | 19.5 | 16.3 | 16.7 | 18.5 |

sea level pressure field over 20°–70°N is $r = 0.87$. As discussed in the previous section, the NBAM index is defined as the leading PC time series of the eddy kinetic energy associated with zonal wavenumbers 4 and higher. The NBAM index explains 43% of the variance in NH synoptic-scale eddy kinetic energy, and both the NAM and NBAM indices are statistically distinct from the second PCs of their respective fields (the variances explained by all PCs considered in this study are listed in Table 1). The positive polarity of the NBAM is defined as periods when the hemispheric mean eddy kinetic energy is anomalously positive, and vice versa. The positive polarity of the NAM is defined as periods when the zonal flow at ~55°N is anomalous westerly, and vice versa. Unless otherwise noted, the fields regressed on the NBAM and NAM indices are *not* filtered.

The NAM and NBAM indices are only weakly correlated at all lags between −20 and +20 days (not shown) and in 10-day low-pass data (Table 2). Roughly 98% of the variance in the NAM on time scales longer than 10 days is linearly independent of variability in the NBAM.

### a. Reviewing the signature of the NAM in the zonal-mean tropospheric circulation

The signature of the NAM in the zonal-mean circulation has been examined extensively in previous work (e.g., Thompson and Wallace 2000; Limpasuvan and Hartmann 2000; Lorenz and Hartmann 2003), but is reviewed here for two reasons: 1) to facilitate comparison with the NBAM and 2) to highlight the surprisingly weak signature of the NAM in the eddy fluxes of heat and eddy kinetic energy.

The left column in Fig. 2 reviews the structure of the NAM in the latitude–height plane. The NAM is marked by meridionally banded anomalies in the zonal-mean zonal flow, with primary centers of action located at ~30° and ~55°N (Fig. 2a; Thompson and Wallace 2000; Limpasuvan and Hartmann 2000). It is also linked to a third center of action in the zonal flow near 75°N (contours in Fig. 2a). However, the center of action near 75°N is restricted to the region to the north of Iceland (not shown), is not evident in regressions based on the leading PC of the monthly-mean sea level pressure (Thompson and Wallace 2000) or zonal wind (Lorenz and Hartmann 2003), and is not clearly mirrored in regressions based on the SAM (e.g., TW). The center of action near 75°N is much weaker when the time series used to generate Fig. 2a are 30-day low-pass filtered, and is thus mainly associated with NAM-like variability on submonthly time scales.

As reviewed in the left column of Fig. 2, the NAM is also associated with 1) poleward momentum fluxes centered near the tropopause ~45°N (shading in Fig. 2a; Limpasuvan and Hartmann 2000; Lorenz and Hartmann 2003), 2) negative temperature anomalies at subpolar latitudes juxtaposed against warm temperature anomalies at middle latitudes (shading in Fig. 2c; Thompson and Wallace 2000), and 3) paired meridional overturning cells with rising motion at subpolar and tropical latitudes juxtaposed against sinking motion between about 30° and 40°N (contours in Fig. 2c). The momentum flux anomalies precede the zonal wind anomalies by several days, consistent with forcing of the zonal-mean flow by the advection of momentum by the eddies (Fig. 3a; Lorenz and Hartmann 2003). The temperature anomalies associated with the NAM are consistent with adiabatic expansion and compression driven by the attendant changes in vertical motion. The vertical motion anomalies, in turn, are consistent with forcing by the momentum fluxes aloft (Thompson and Wallace 2000). Note that the mass streamfunction has very small

TABLE 2. Correlations between the leading PCs of the fields indicated. The PCs are described in association with Table 1. Correlations are computed between 10-day low-pass-filtered versions of the PC time series. All results are significant at the 99% confidence level based on a two-tailed test of the *t* statistic.

| | PC1 $EKE_{WN4+}$ (NBAM) | PC1 ZKE | PC1 *U* (NAM) |
|---|---|---|---|
| PC1 $EKE_{WN4+}$ (NBAM) | 1 | 0.15 | 0.15 |
| PC1 ZKE | 0.15 | 1 | 0.85 |

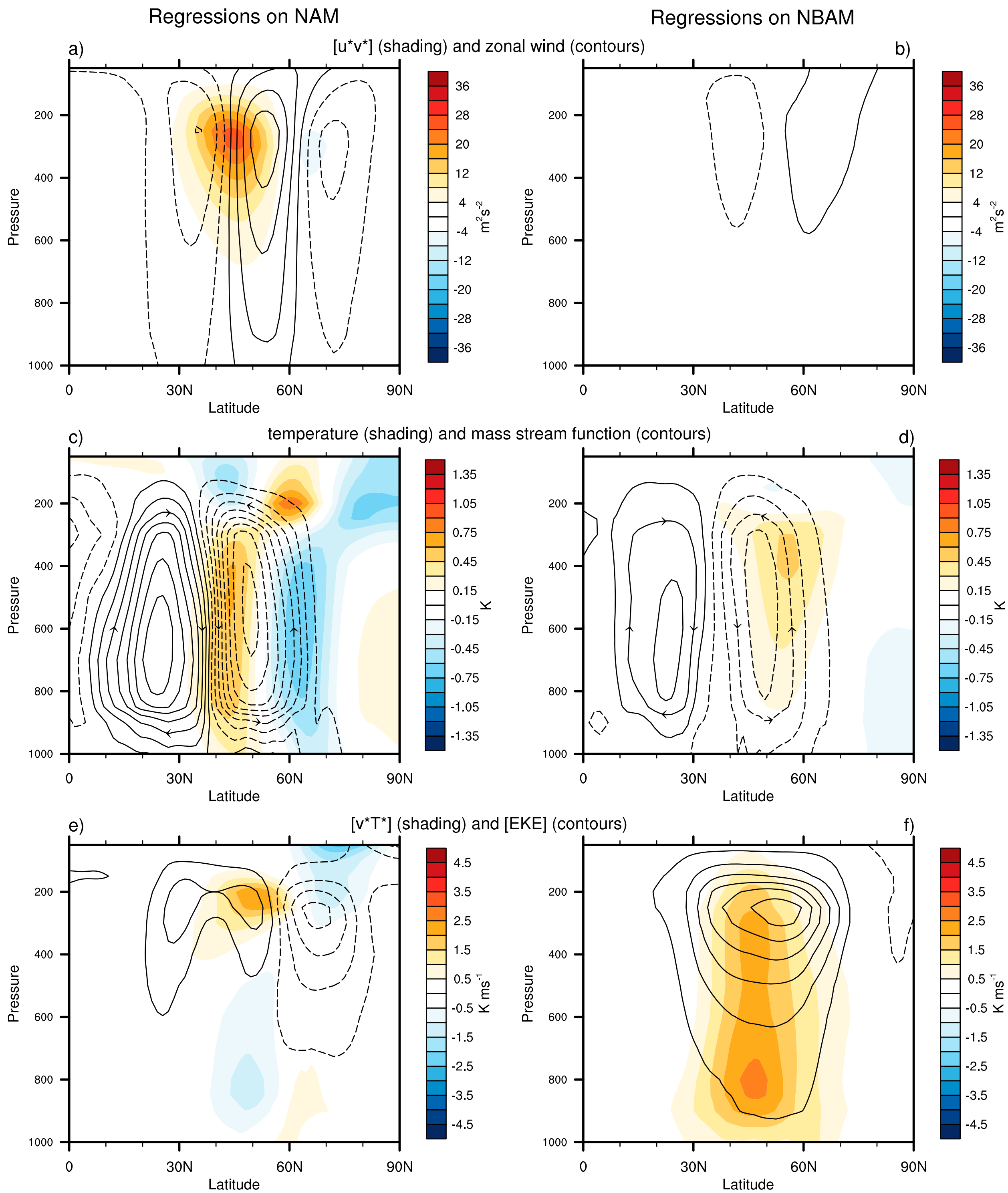


FIG. 2. Vertical structure of the northern annular mode (NAM) and northern baroclinic annular mode (NBAM) in the zonal-mean circulation. Results show daily-mean, zonal-mean values of the fields indicated regressed on standardized values of the (a),(c),(e) NAM and (b),(d),(f) NBAM indices: (top)–(bottom) $[u^*v^*]$ (shading) and $[U]$ (contours); $[T]$ (shading) and mass streamfunction (contours); and $[v^*T^*]$ (shading) and [EKE] (contours). The NAM index is defined as the leading PC time series of NH zonal-mean zonal wind. The NBAM index is defined as the leading PC of NH synoptic-scale zonal-mean eddy kinetic energy. Results are based on daily-mean data for all calendar months. Regression coefficients are based on contemporaneous values of the data, except in the cases of $[u^*v^*]$ and $[v^*T^*]$, in which the fluxes lead the NAM and NBAM indices by 1 day. Contours are at (top) $-0.5, 0.5, 1.5\ \mathrm{m\,s^{-1}}$, etc.; (middle) $-0.5, 0.5, 1.5 \times 10^9\ \mathrm{kg\,s^{-1}}$, etc.; and (bottom) $-3, 3, 9\ \mathrm{m^2\,s^{-2}}$, etc. Solid and dashed contours denote clockwise and counterclockwise motion in (middle).

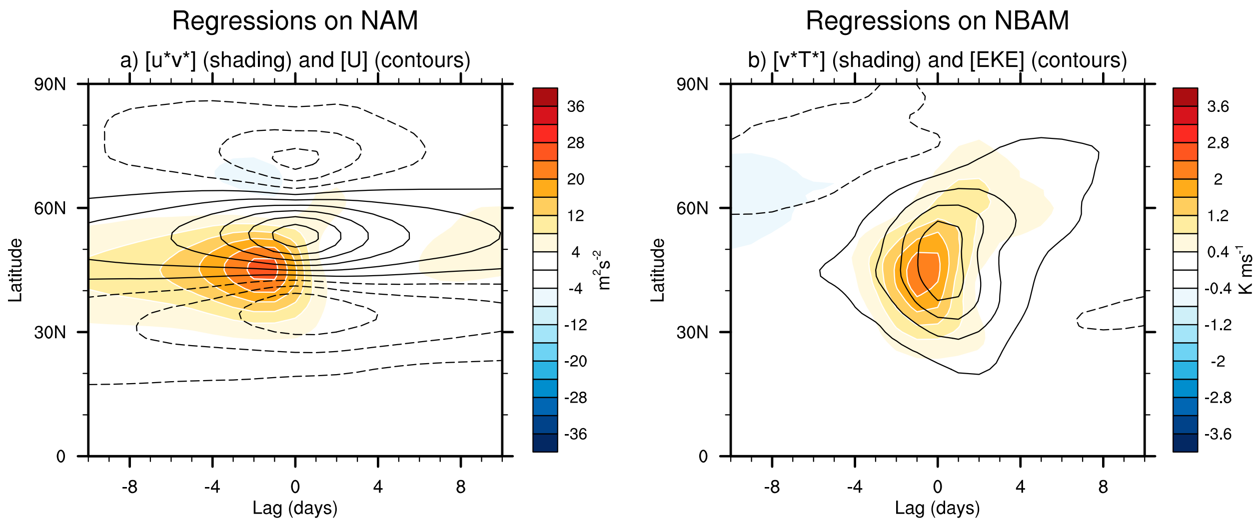


FIG. 3. Latitude–lag structure of the (a) NAM and (b) NBAM. Results show daily-mean, zonal-mean values of the fields indicated regressed on standardized values of the NAM and NBAM indices as a function of latitude and lag. The momentum fluxes, zonal wind, and EKE are shown at 300 hPa. The heat fluxes are shown at 850 hPa. Negative lags denote the field leads the base index and vice versa. Contours are at (left) −0.35, 0.35, 1.5 m s$^{-1}$, etc., and (right) −3.5, 3.5, 10.5 m$^2$ s$^{-2}$, etc.

amplitude at high latitudes in part due to the relatively small area represented by the polar cap (Fig. 2c).

The signatures of the NAM in the zonal wind and eddy fluxes of momentum discussed above are consistent with north–south fluctuations in the axis of the extratropical jet (Lorenz and Hartmann 2003). The signatures of the NAM in the eddy kinetic energy and eddy heat flux anomalies are more difficult to interpret (Fig. 2e). To the extent that variations in the eddy heat fluxes and eddy kinetic energy follow variations in the latitude of the jet, the positive polarity of the NAM should be accompanied not only by anomalously poleward momentum fluxes in the upper troposphere near 45°N, but also by increases in the eddy fluxes of heat and eddy kinetic energy near 55°N and decreases near 30°N. Neither feature is clearly apparent in Fig. 2e. As is the case for the SAM (TW), the signature of the NAM in the eddy fluxes of heat is both weak and amorphous throughout most of the midlatitudes (Fig. 2e).

The signature of the NAM in the eddy fluxes of heat and momentum is explored further in the left column of Fig. 4. Figure 4a shows the unfiltered eddy fluxes of momentum (contours; reproduced from shading in Fig. 3a) and heat (shading) regressed on the NAM index as a function of lag and latitude. Figures 4c and 4e show the components of the regressions that are due to synoptic (wavenumbers 4 and higher) and planetary-scale (wavenumbers 1–3) waves, respectively. Note that in contrast to the diagnostics presented in DeWeaver and Nigam (2000), Feldstein (2003), and Lorenz and Hartmann (2003), the wave fluxes in Fig. 4 are spatially rather than time filtered.

As evidenced in Figs. 4c and 4e, the preponderance of the eddy momentum flux anomalies associated with the NAM are due to variations in synoptic-scale waves. In contrast, a large fraction of the eddy heat flux anomalies associated with the NAM are due to variations in the planetary-scale waves (Fig. 4e), particularly the meridional dipole in eddy heat flux anomalies centered around lag 0. The most pronounced signature of the NAM in the synoptic-scale wave fluxes of heat is found at a positive lag near 50°N (Fig. 4c), and is consistent with the influence of the momentum fluxes aloft on lower-tropospheric baroclinicity (Lorenz and Hartmann 2003).

### b. *The signature of the NBAM in the zonal-mean tropospheric circulation*

The structure of the NBAM in the extratropical circulation is shown in the right columns of Figs. 2–4. In contrast to the NAM but like its SH counterpart (TW), the NBAM has a weak signature in the zonal-mean zonal wind and wave fluxes of momentum (Fig. 2b) but a pronounced signature in the zonal-mean eddy kinetic energy and wave fluxes of heat (Fig. 2f). Hence, the NBAM is associated with hemispheric-scale fluctuations in both the generation of eddy kinetic energy in the lower troposphere (as inferred by the vertical gradient in the eddy fluxes of heat near the surface) and eddy amplitudes aloft (as inferred by the eddy kinetic energy). The eddy heat flux anomalies precede the eddy kinetic energy anomalies by ~1–2 days, consistent with the generation of upper-tropospheric eddy kinetic energy by developing baroclinic waves in the free troposphere (Fig. 3b; Simmons and Hoskins 1978).

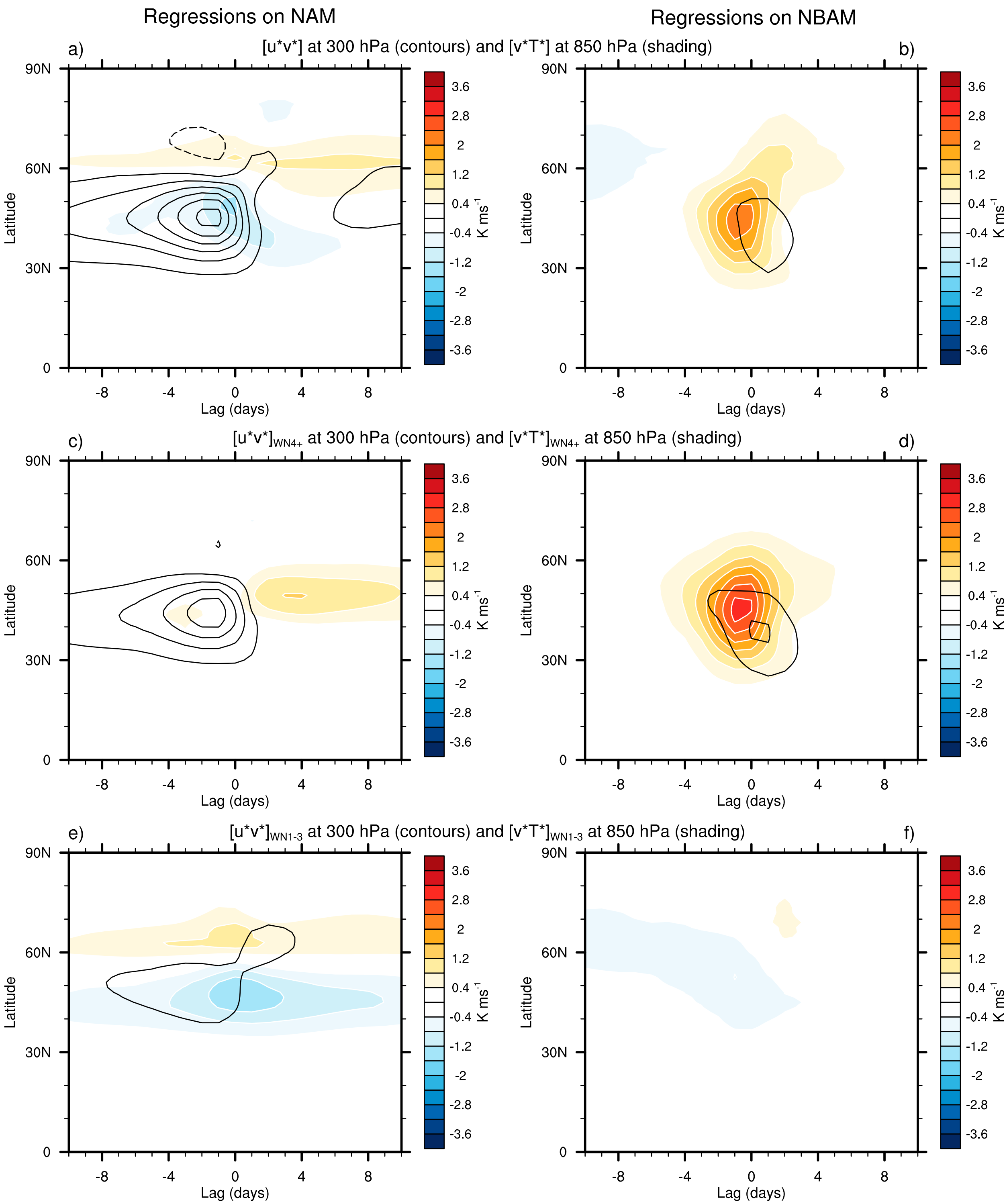


FIG. 4. Wavenumber breakdown of the latitude–lag structure of the (left) NAM and (right) NBAM in the eddy fluxes of heat $[v^*T^*]$ (shading) and momentum $[u^*v^*]$ (contours). Results show daily-mean, zonal-mean values of the fields indicated regressed on standardized values of the NAM and NBAM indices as a function of latitude and lag. (top) Unfiltered data (reproduced from the corresponding results in Fig. 3). (middle),(bottom) The components of the regressions in the (top) that are due to synoptic- (zonal wavenumbers $\geq$ 4) and planetary-scale (zonal wavenumbers 1–3) waves, respectively. Negative lags denote the field leads the base index, and vice versa. The contour interval is 4 $m^2 s^{-2}$.

Also like its SH counterpart (TW), the NBAM is marked by warm temperature anomalies centered near 50°–60°N (shading in Fig. 2d) that are consistent with warming by the anomalously poleward wave fluxes of heat at the midlatitudes (shading in Fig. 2f). In contrast to the NAM, the changes in vertical motion are thermally driven (i.e., thermally direct): the midlatitude temperature anomalies are damped rather than driven by the vertical motion anomalies (contours in Fig. 2d).

In part by construction, the anomalous eddy fluxes of heat and momentum associated with the NBAM are dominated by synoptic-scale eddies (right column in Fig. 4). Consistent with the barotropic decay stage of baroclinic waves (Simmons and Hoskins 1978), the NBAM is marked by positive anomalies in the wave fluxes of momentum that lag and lie slightly equatorward of the positive anomalies in the wave fluxes of heat (Fig. 4d).

### c. Summarizing the differences between the NAM and NBAM

As is the case in the SH, the barotropic (the NAM) and baroclinic (the NBAM) northern annular modes have very different signatures in the extratropical circulation. The NAM emerges as the leading PC of the zonal-mean kinetic energy (Table 2). It is driven by the wave fluxes of momentum (Fig. 3a), and has a weak secondary signature in the synoptic-scale wave fluxes of heat that is consistent with the influence of the momentum fluxes upon tropospheric baroclinicity (Fig. 4c; Lorenz and Hartmann 2003). Hence, the NAM explains a large fraction of the variance in the zonal-mean zonal wind and eddy fluxes of momentum (left panels in Fig. 5; solid lines), but a relatively small fraction of the variance in the zonal-mean eddy kinetic energy and eddy fluxes of heat (left panels in Fig. 5; dashed lines).

In contrast, the NBAM emerges as the leading EOF of the eddy kinetic energy. It is driven by the wave fluxes of heat (Fig. 3b), and has a secondary signature in the wave fluxes of momentum that is consistent with the baroclinic wave life cycle (Fig. 4d). Hence, the NBAM explains a notable fraction of the variance in the zonal-mean eddy kinetic energy and eddy fluxes of heat (right panels in Fig. 5; dashed lines), but a very small fraction of the variance in the zonal-mean zonal wind and eddy fluxes of momentum (right panels in Fig. 5; solid lines). The NBAM explains a smaller fraction of the variance in the eddy kinetic energy than the NAM does in the zonal-mean kinetic energy (Figs. 5c,d).

The results shown in this section are based on data for all calendar months. The NBAM also emerges as the leading PC of synoptic-scale eddy kinetic energy in analyses performed separately for the warm- and cold-season months. For example, the correlations between 1) warm-season (April–September) segments of the year-round NBAM index and 2) the leading PC of warm-season synoptic-scale eddy kinetic energy is $r \sim 0.99$. As is the case for the NAM (Thompson and Wallace 2000), the amplitude of the NBAM is largest during the cold-season months.

In the following section, we will examine the signature of the NBAM in the longitudinally varying circulation and assess the linkages between synoptic-scale eddy kinetic activity in the North Atlantic and North Pacific sectors of the hemisphere.

## 5. Longitudinally varying aspects of the NBAM

The robust signatures of both the NH and SH baroclinic annular modes in the zonal-mean circulation suggest that they owe their existence to dynamical processes that transcend the land–sea contrasts of their respective hemispheres. In this section, we examine three aspects of the NBAM in the longitudinally varying circulation: 1) its signature in eddy activity and precipitation, 2) its emergence as the leading pattern of variability in eddy kinetic energy along latitude circles, and 3) its signature in the teleconnectivity between eddy kinetic energy in the two major NH storm-track regions.

### a. The signature of the NBAM in the longitudinally varying circulation

Figure 6 shows three zonally varying, daily-mean fields regressed onto standardized daily-mean values of the NBAM index: the eddy kinetic energy at the 300-hPa level (Fig. 6a), the eddy heat fluxes at the 850-hPa level (Fig. 6b), and precipitation (Fig. 6c). The eddy heat flux and precipitation results are lagged by $-1$ day relative to the NBAM index [i.e., the fields peak $\sim$1 day before eddy kinetic energy peaks in the upper troposphere; see Fig. 3b and also Thompson and Barnes (2014)]. As in Figs. 2 and 3, the eddy fields shown in Fig. 6 are not spatially filtered. The ERA-Interim precipitation is a model-derived quantity but is assumed to provide a physically consistent, zeroth-order estimate of the linkages with variability in the NBAM.

As evidenced in Fig. 6, the positive polarity of the NBAM is associated with anomalously positive eddy kinetic energy, poleward eddy heat fluxes, and enhanced precipitation over both the North Pacific and North Atlantic sectors of the hemisphere. Over the Pacific sector, the eddy kinetic energy anomalies peak over the Kuroshio extension region and the central North Pacific, whereas the heat flux anomalies peak over the central and eastern North Pacific. Over the Atlantic sector, the eddy kinetic energy and eddy heat flux anomalies peak over the Gulf Stream extension region. Precipitation is enhanced primarily over the Kuroshio and Gulf Stream extension regions.

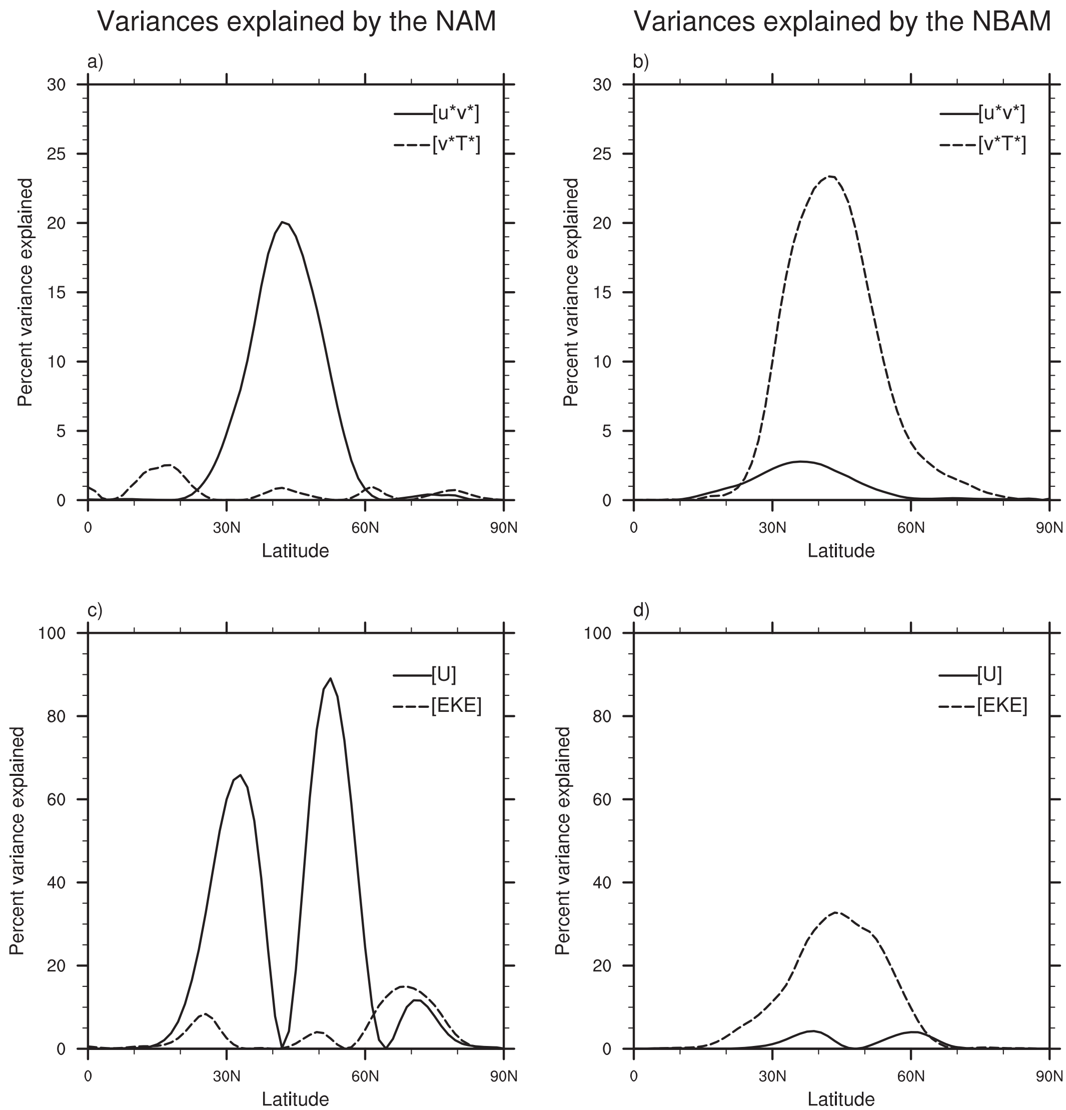


FIG. 5. Percent variance explained by the (a),(c) NAM and (b),(d) NBAM in vertically averaged values of the indicated fields: (top) $[u^*v^*]$ and $[v^*T^*]$ and (bottom) $[U]$ and [EKE]. The time series and data are 10-day low-pass filtered to emphasize covariability on time scales longer than those associated with a typical baroclinic wave. The fields are vertically averaged between 950 and 250 hPa.

Figure 6 reveals that variability in the NBAM is marked by variations in eddy activity that span both major storm-track regions. In section 5b, we will examine whether the large-scale structure of the NBAM is an artifact of the use of zonal-mean data to define the NBAM index, or whether it also emerges from PC analysis of eddy kinetic energy anomalies along latitude circles.

### b. *PC analysis of the longitudinally varying circulation along latitude circles*

Figure 7c shows the correlations between 1) the leading PC time series of the longitudinally varying, synoptic-scale eddy kinetic energy calculated as a function of latitude (e.g., at 50°N, the leading PC is calculated for eddy kinetic energy anomalies associated with wavenumbers 4 and higher along 50°N as a function of time and longitude); and 2) the NBAM index. Figure 7d shows the corresponding variances explained by the first two PCs of the longitudinally varying synoptic-scale eddy kinetic energy as a function of latitude, where the error bars correspond to the criterion outlined in North et al. (1982). For example, the leading PC of the longitudinally varying synoptic-scale eddy kinetic energy along 50°N is well separated from the second PC at 50°N (Fig. 7d), and is correlated with the NBAM index at

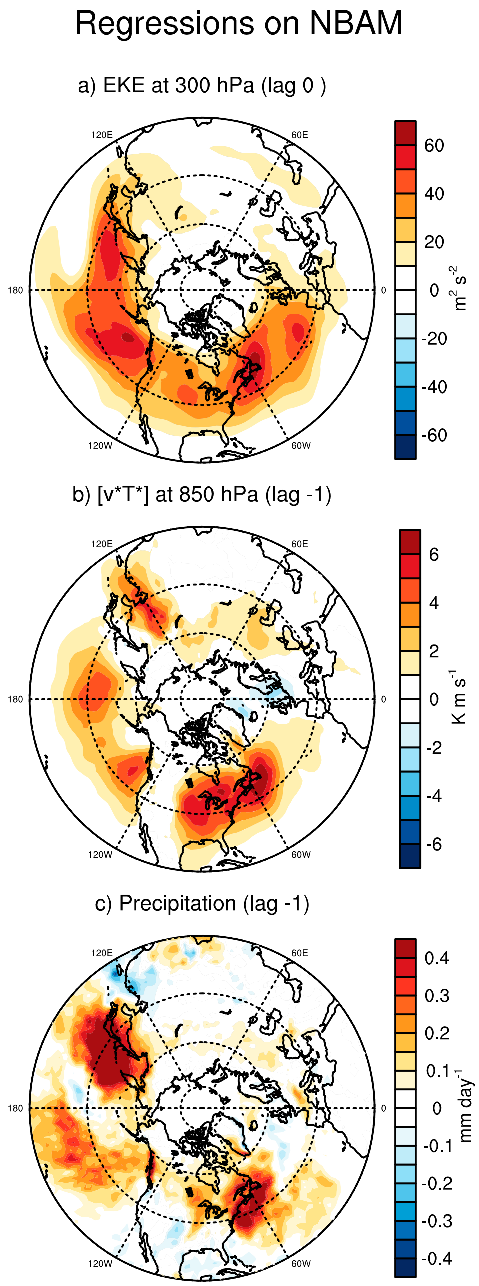


FIG. 6. Horizontal structure of the NBAM in EKE, eddy fluxes of heat, and precipitation. Results show (a) daily-mean eddy kinetic energy at 300 hPa, (b) the eddy fluxes of heat at 850 hPa, and (c) precipitation regressed onto standardized values of NBAM index. The heat fluxes and precipitation lead the NBAM index by 1 day.

a level of $r \sim 0.8$ (Fig. 7c). Figures 7a and 7b show corresponding results for the longitudinally varying zonal wind field and the NAM index.

The leading PCs of the longitudinally varying synoptic-scale eddy kinetic energy field are highly correlated with the NBAM index throughout the midlatitudes (right panels in Fig. 7). Likewise, the leading PCs of the longitudinally varying zonal wind field are strongly correlated with the NAM index time series at latitudes that lie within the primary centers of action of the NAM (left panels in Fig. 7). Hence, the NAM and NBAM correspond to the leading patterns of variability in the longitudinally varying circulation along latitude circles, and are not an artifact of the zonal averaging performed before calculating the NAM and NBAM indices.

### *c. Teleconnectivity in eddy kinetic energy between storm tracks*

The NBAM exhibits a notable degree of annularity in the eddy kinetic energy field (Fig. 6). In practice, two conditions can lead to an annular-like leading PC in the atmospheric circulation: 1) fluctuations in the circulation must be positively correlated at adjacent grid boxes (though not necessarily between widely separate longitudes) and 2) the variance of the circulation must exhibit a high degree of zonal symmetry (Gerber and Vallis 2005). Neither condition requires zonally coherent fluctuations in the flow; hence, an annular-like leading PC can arise even in the absence of significant positive correlations between variability in the circulation over the two storm-track regions. In a companion study (E. P. Gerber and D. W. J. Thompson 2014, unpublished manuscript), we examine the conditions under which the NBAM reflects zonally coherent fluctuations in the flow. Below we examine the structure of the NBAM over both major NH storm-track regions and explore the teleconnectivity in eddy kinetic energy between them.

First, we examine to what extent the structure of the NBAM emerges from analyses of the circulation over the North Atlantic and North Pacific sectors of the hemisphere. The results in Fig. 8 are identical to those shown in the right column of Fig. 2, but are derived from analyses restricted to 90°W–50°E (the North Atlantic sector) and 110°E–110°W (the North Pacific sector). For example, the $\mathrm{NBAM_{Atlantic}}$ index is defined as the leading PC of the synoptic-scale eddy kinetic energy from 1000 to 200 hPa averaged for 90°W–50°E, and the results in the left column of Fig. 8 show unfiltered data averaged for 90°W–50°E regressed on standardized values of the $\mathrm{NBAM_{Atlantic}}$ index. The right column shows analogous results calculated for the North Pacific sector. The results in Fig. 8 are not sensitive to the specific boundaries used to designate the Pacific and Atlantic sectors of the hemisphere.

The key result in Fig. 8 is that the leading patterns of variability in the amplitude of synoptic-scale eddy activity in the Atlantic and Pacific sectors of the NH both bear a strong resemblance to the NBAM. Both are marked by a monopole in the eddy fluxes of heat and eddy kinetic energy centered at ~40°–50°N (Figs. 8e,f;

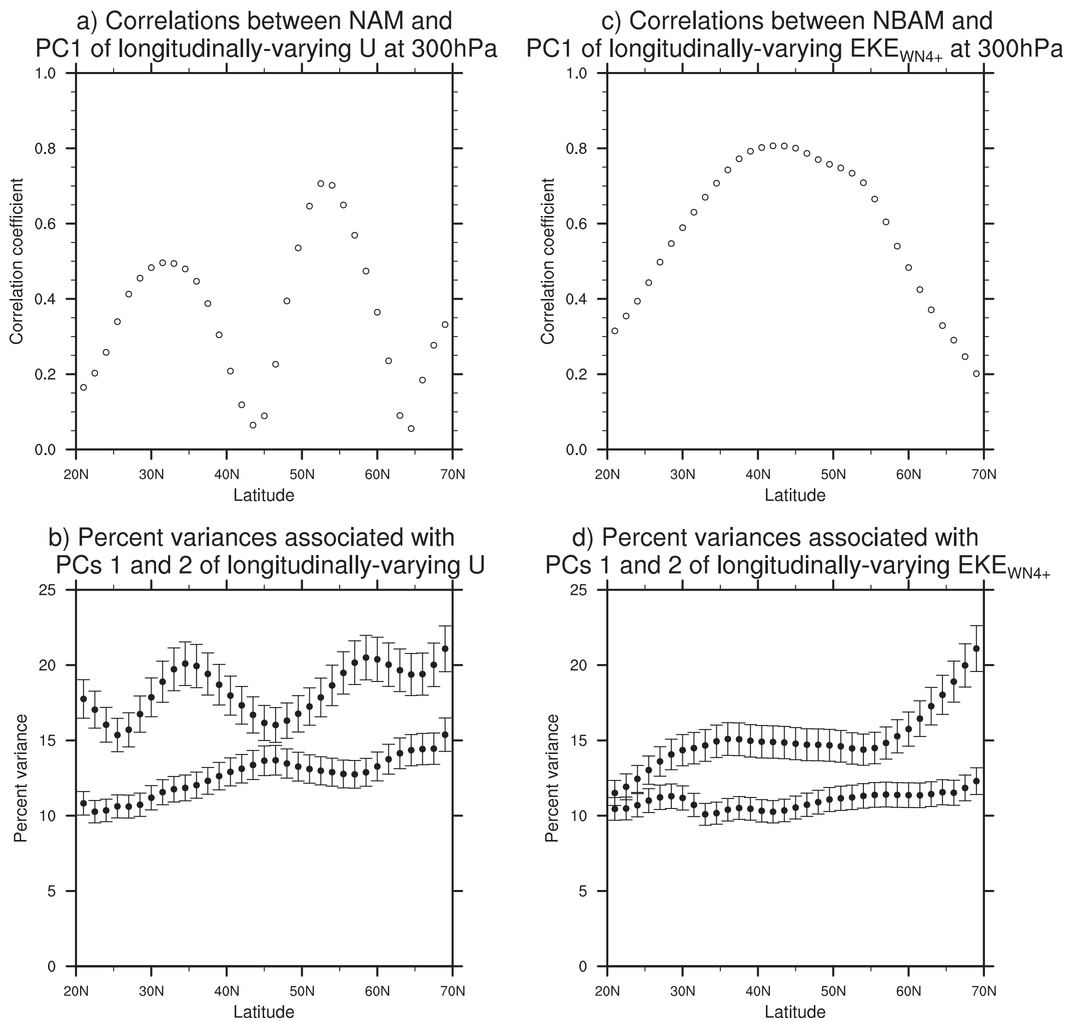


FIG. 7. (a) Correlations between the NAM index and the leading PCs of the daily-mean, longitudinally varying zonal wind. The PCs are calculated as a function of latitude. (b) Variances explained by the first and second PCs of the daily-mean, longitudinally varying zonal wind. (c) As in (a), but for correlations between the NBAM index and the leading PCs of daily-mean, synoptic-scale eddy kinetic energy. (d) As in (b), but for the PCs of the daily-mean, synoptic-scale eddy kinetic energy. Error bars in (c),(d) are derived from the significance test described in North et al. (1982). The PCs are calculated based on daily-mean data. The correlations are based on 10-day low-pass versions of the time series to emphasize covariability on time scale longer than those associated with a typical baroclinic wave.

the eddy kinetic energy anomalies associated with the NBAM$_{\mathrm{Atlantic}}$ index are shifted slightly poleward of their Pacific counterparts), both exhibit positive temperature anomalies that peak ~400 hPa near 50°N (Figs. 8c,d), and both have a relatively weak signature in the zonal wind field (Figs. 8a,b). The similarities between the leading modes of eddy kinetic energy over the two storm-track regions is surprising considering the notable differences in the climatology of the two sectors.

The NBAM$_{\mathrm{Atlantic}}$ and NBAM$_{\mathrm{Pacific}}$ indices are correlated with the NBAM index at levels of $r = 0.67$ and $r = 0.72$, respectively. Hence, they contribute roughly equally to variations in the NBAM index. The NBAM$_{\mathrm{Atlantic}}$ and NBAM$_{\mathrm{Pacific}}$ indices are also significantly linked to each other. Figure 9 shows the correlations between the NBAM$_{\mathrm{Atlantic}}$ and NBAM$_{\mathrm{Pacific}}$ indices as a function of lag. The leading patterns of synoptic-scale eddy kinetic energy over the North Pacific sector and North Atlantic sector are significantly linked to each other, particularly when the North Pacific sector leads the North Atlantic sector by ~3–4 days. The correlations between the two sectors are most pronounced during the cold-season months (not shown).

The linkages between eddy kinetic energy in the two storm-track regions are further evidenced in the lag

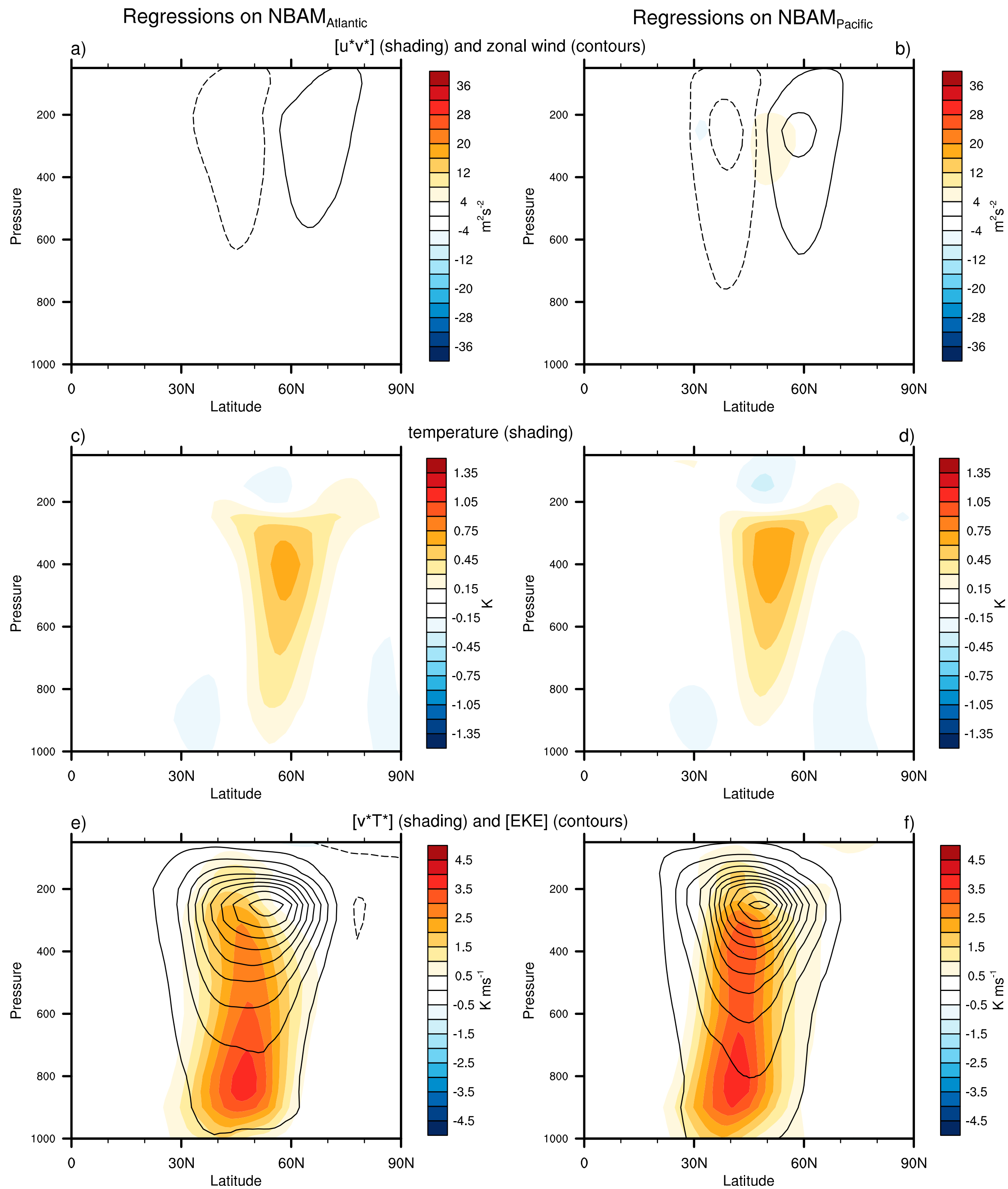


FIG. 8. Structure of baroclinic annular variability over the North Atlantic and North Pacific sectors of the hemisphere. As in the right column of Fig. 2, but for results calculated separately for the (a),(c),(e) Atlantic (90°W–50°E) and (b),(d),(f) Pacific (110°E–110°W) sectors of the hemisphere: (top) $[u^*v^*]$ (shading) and $[U]$ (contours); (middle) $[T]$ (shading); and (bottom) $[v^*T^*]$ (shading) and [EKE] (contours). (Brackets denote sectoral rather than zonal averages.) The NBAM$_{\mathrm{Atlantic}}$ is defined as the leading PC time series of synoptic-scale EKE in the Atlantic sector from 1000 to 200 hPa and the NBAM$_{\mathrm{Pacific}}$ index, as the leading PC time series of synoptic-scale EKE in the Pacific sector from 1000 to 200 hPa.

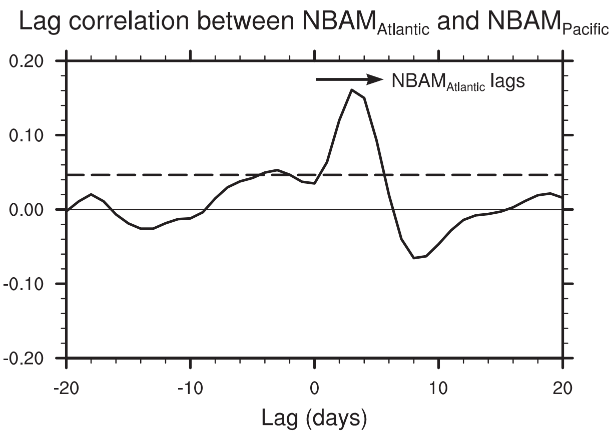


FIG. 9. Lead–lag correlations between the NBAM$_{Pacific}$ index and NBAM$_{Atlantic}$ index. Negative lags denote the NBAM$_{Atlantic}$ index leads the NBAM$_{Pacific}$, and vice versa. The horizontal dashed line indicates the 99% significance level based on a two-tailed test of the $t$ statistic.

regressions of (unfiltered) eddy kinetic energy at the 300-hPa level onto the NBAM$_{Pacific}$ index. At lag 0 (Fig. 10a), the eddy kinetic energy anomalies associated with the NBAM$_{Pacific}$ index have large amplitude over the Pacific sector but do not project onto eddy kinetic energy over the North Atlantic sector. At successive lags, the eddy kinetic anomalies not only decay over the Pacific sector, but also appear to propagate across North America toward the North Atlantic in a manner consistent with that shown in Chang and Yu (1999) and Li and Lau (2012). Roughly ~3–4 days after peak amplitude in the NBAM$_{Pacific}$ index (Figs. 10d,e), the North Atlantic storm track is marked by positive—albeit relatively weak—anomalies in eddy kinetic energy centered over the Gulf Stream extension region. The linkages between eddy kinetic energy in the Pacific sector and over the Gulf Stream extension region ~3–4 days later are statistically significant at the 99% confidence level (Figs. 10d,e and 11). The downstream development of eddy kinetic energy anomalies across Asia toward the North Pacific is much less clear (not shown).

Several studies have argued that variations in upper-tropospheric baroclinic activity in the two storm tracks are significantly correlated (e.g., Chang and Fu 2002; Chang 2004; Li and Lau 2012). But others have noted that the correlations between the storm tracks are very weak (Wettstein and Wallace 2010). The results shown in Figs. 9–11 confirm that the linkages between upper-tropospheric variability in the storm tracks are weak. But they also confirm that the linkages are significant, particularly when the North Pacific storm track leads the North Atlantic storm track by several days. To what extent the weak but significant propagation of eddy kinetic

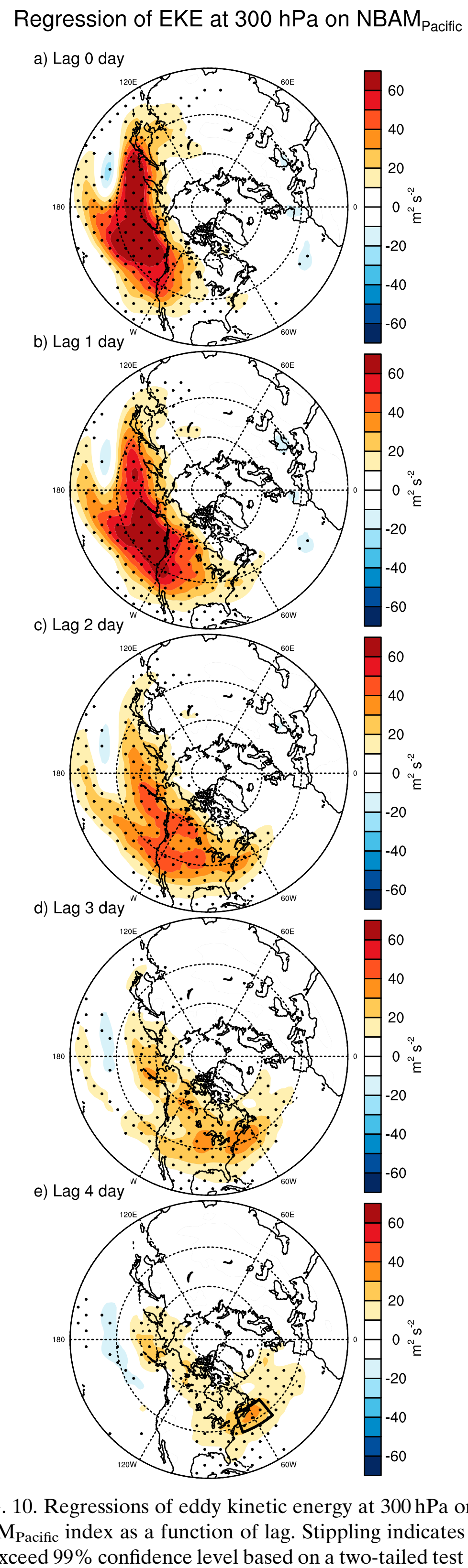


FIG. 10. Regressions of eddy kinetic energy at 300 hPa onto the NBAM$_{Pacific}$ index as a function of lag. Stippling indicates results that exceed 99% confidence level based on a two-tailed test of the $t$ statistic: (a)–(e) lags 0, 1, 2, 3, and 4 days, respectively.

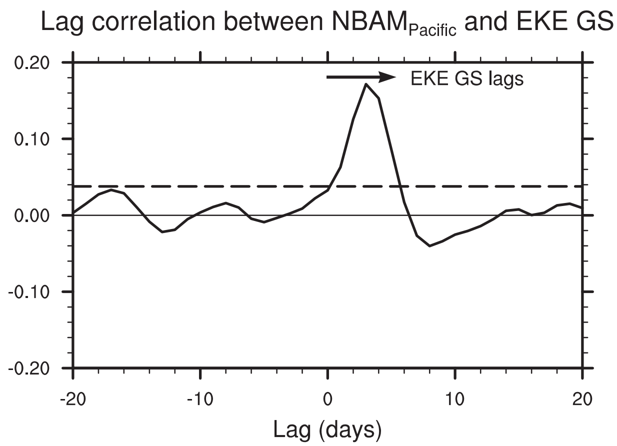


FIG. 11. As in Fig. 9, but for lead–lag correlations between the $NBAM_{Pacific}$ index and eddy kinetic energy at 300 hPa averaged over the Gulf Stream extension region (see black borders indicated in Fig. 10e). Horizontal line indicates 99% significance levels based on a two-tailed test of the $t$ statistic.

energy from the North Pacific to North Atlantic storm tracks contributes to the zonally symmetric structure of the NBAM is examined in the companion study (E. P. Gerber and D. W. J. Thompson 2014, unpublished manuscript).

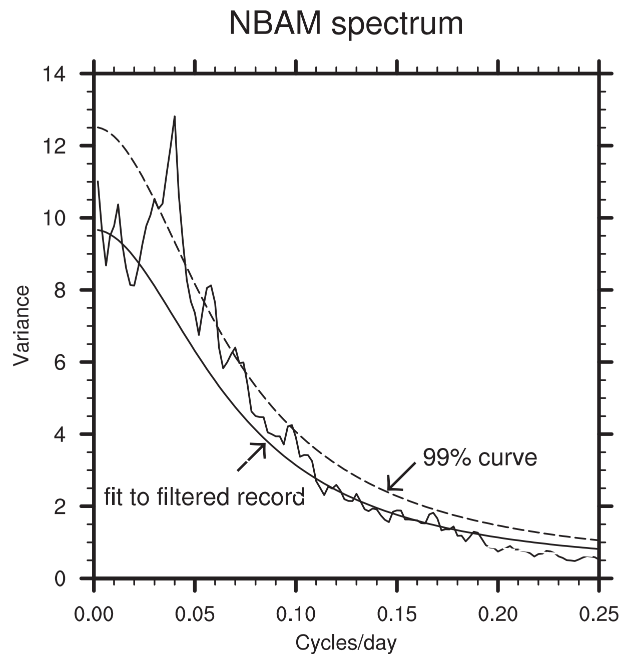


FIG. 12. Power spectra of the NBAM index calculated from daily-mean data for all calendar days. The solid smooth curve is the red noise fit to the 20-day high-pass-filtered NBAM index and the dashed smooth curve is the 99% confidence level. See text and the appendix for details of the calculation.

## 6. Quasi-periodic behavior in the NBAM

The southern baroclinic annular mode exhibits quasi-periodic variability on time scales of ~20–30 days (TW). The quasi-periodic behavior in the SBAM is consistent with two-way feedbacks between the extratropical baroclinicity and the eddy fluxes of heat by baroclinic waves, and extends to large-scale averages of eddy kinetic energy, the eddy fluxes of heat, and precipitation (Thompson and Barnes 2014). Below we investigate to what extent analogous quasi-periodic behavior is evident in association with the NBAM.

Figure 12 shows the power spectrum of the NBAM index calculated for data for all calendar months (details of the calculation are provided in section 2). The NBAM index time series exhibits enhanced spectral power centered around ~25 days (~0.04 cpd). The peak in the spectrum is weaker than the corresponding peak in the SBAM (TW, cf. Fig. 12). But it is reproducible in subsets of the data (see Fig. A1 in the appendix) and is statistically significant at the 99% level based on the chi-squared statistic applied to a red-noise fit to the spectrum (see section 2 and the appendix for details of the significance tests). Interestingly, the spectral peak in the NBAM index derives almost entirely from the summer season, as evidenced in the top panels in Fig. 13. Both the pronounced spectral peak during summer and the lack of a robust peak during winter are reproducible in both halves of the data record (see Fig. A1 in the appendix). The lack of a robust peak during the cold season is consistent with Ambaum and Novak (2014), who did not find evidence of statistically significant periodicity in the North Atlantic storm track during the winter season.

The spectral peak in the NBAM during the warm-season months extends to various indices of synoptic eddy activity. It is apparent in the spectrum of the hemispheric-mean synoptic-scale eddy kinetic energy at 300 hPa (not shown; the spectrum is largely identical to that for the NBAM index). And it is apparent in the spectrum of the hemispheric-mean eddy fluxes of heat by synoptic-scale eddies (Fig. 13c).

The spectral peak in the NBAM is statistically significant, reproducible in subsets of the data, and evident in the eddy fluxes of heat. However, for the most part, it is less robust than its SH counterpart. The peak in the NBAM and its seasonality are not reproducible in the same coupled atmosphere–ocean climate model that readily simulates the peak in the SBAM [the Geophysical Fluid Dynamics Laboratory (GFDL) Coupled Climate Model version 3 (CM3); Thompson and Barnes (2014)]. The peak in the NBAM is not

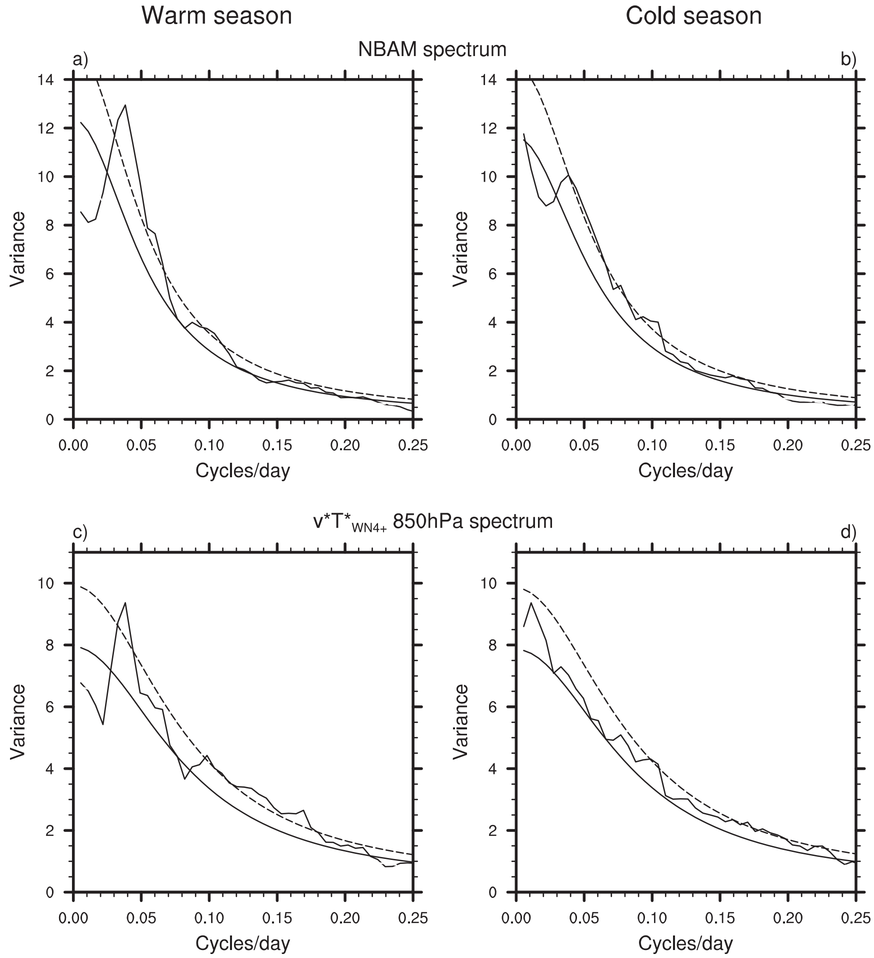


FIG. 13. Power spectra of (a),(b) the NBAM index and (c),(d) the synoptic-scale eddy fluxes of heat at 850 hPa averaged over 30°–70°N. Results are calculated based on daily-mean data during the (left) warm and (right) cold seasons. Warm and cold seasons are defined as April–September and October–March, respectively. Curves are as in Fig. 12, except that the red-noise fit is calculated for 30-day high-pass-filtered data. See text for details of the calculation. Note that the differences in spectral resolution between the results shown in Figs. 12 and 13 are due to the different subset lengths used in the calculations (section 2).

apparent in data restricted to the North Atlantic and North Pacific storm-track regions (i.e., it is not evident in the $\mathrm{NBAM}_{\mathrm{Atlantic}}$ and $\mathrm{NBAM}_{\mathrm{Pacific}}$ indices). And the peak in the NBAM and its seasonality are not clearly reproducible in NH-mean precipitation (the peak in the SBAM clearly extends to SH-mean precipitation; Thompson and Barnes 2014). The spectral peak in the NBAM will be examined in more detail in a companion paper.

## 7. Conclusions

The NBAM is remarkably similar to its SH counterpart despite the pronounced differences in the land–sea geometry of the two hemispheres (Fig. 14). Both are characterized by hemispheric-scale monopoles in the eddy kinetic energy and eddy fluxes of heat (Fig. 14, bottom). Both have very weak signatures in the wave fluxes of momentum and the zonal-mean zonal flow (Fig. 14, top). Also both are associated with changes in vertical motion and temperature that are consistent with the circulation response to the anomalous fluxes of heat (Fig. 14, middle, i.e., the regions poleward of the maximum heat flux anomalies are marked by anomalously warm conditions and anomalous rising motion).

The NBAM is also reminiscent of the leading patterns of storm-track variability identified in previous work. A large-scale monopole in the amplitude of eddy activity also emerges from PC analyses of 1) the variance of the 10-day high-pass-filtered upper-tropospheric meridional

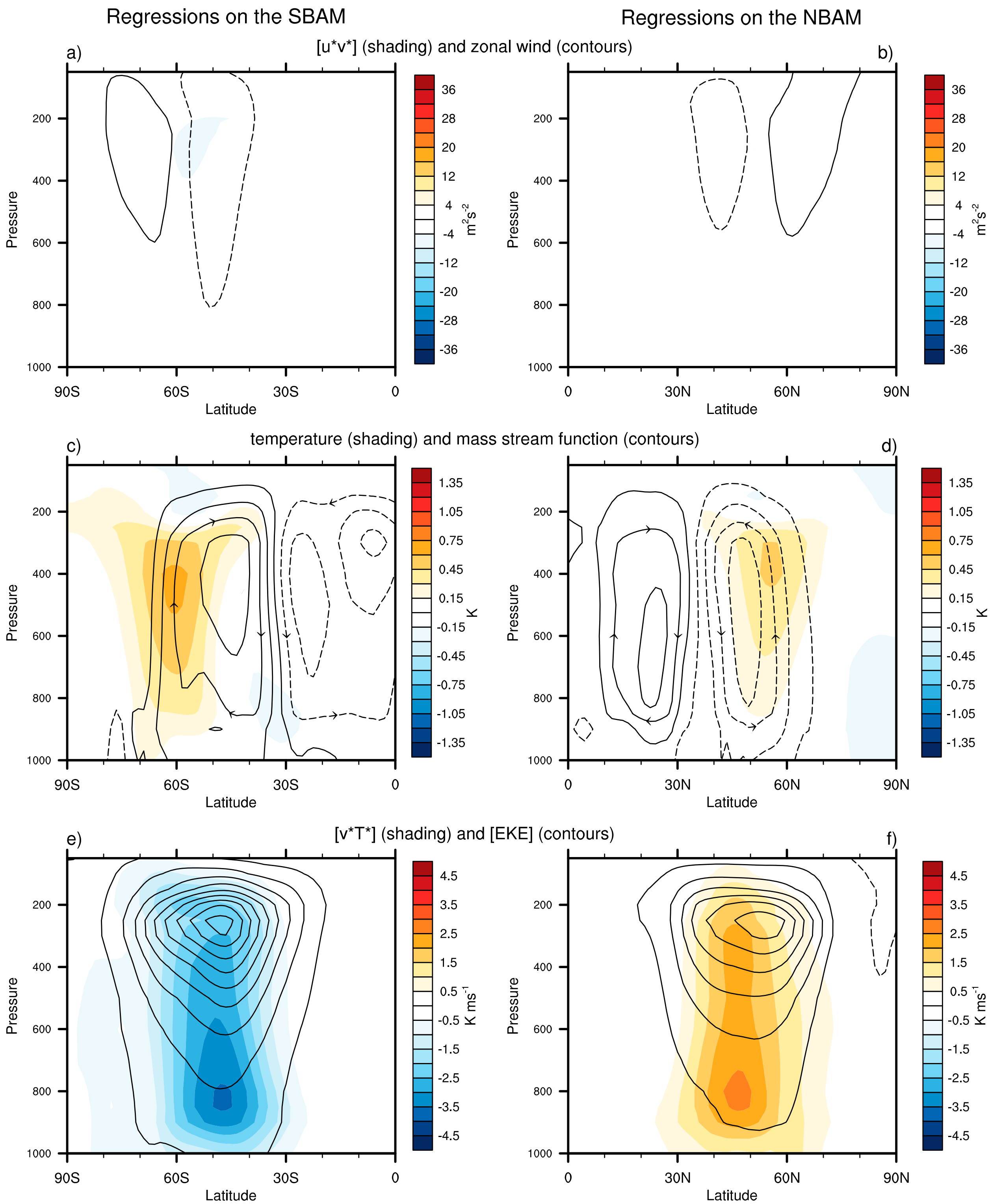


FIG. 14. Comparing the vertical structures of the southern and northern baroclinic annular modes. Results show daily-mean, zonal-mean values of the fields indicated regressed on standardized values of the (a),(c),(e) SBAM and (b),(d),(f) NBAM indices: (top)–(bottom) [$u^*v^*$] (shading) and [$U$] (contours); [$T$] (shading) and mass streamfunction (contours); and [$v^*T^*$] (shading) and [EKE] (contours). Results for the NBAM are reproduced from Fig. 2 (right). Results for the SBAM are reproduced from TW (but based on the period of record January 1979–December 2011).

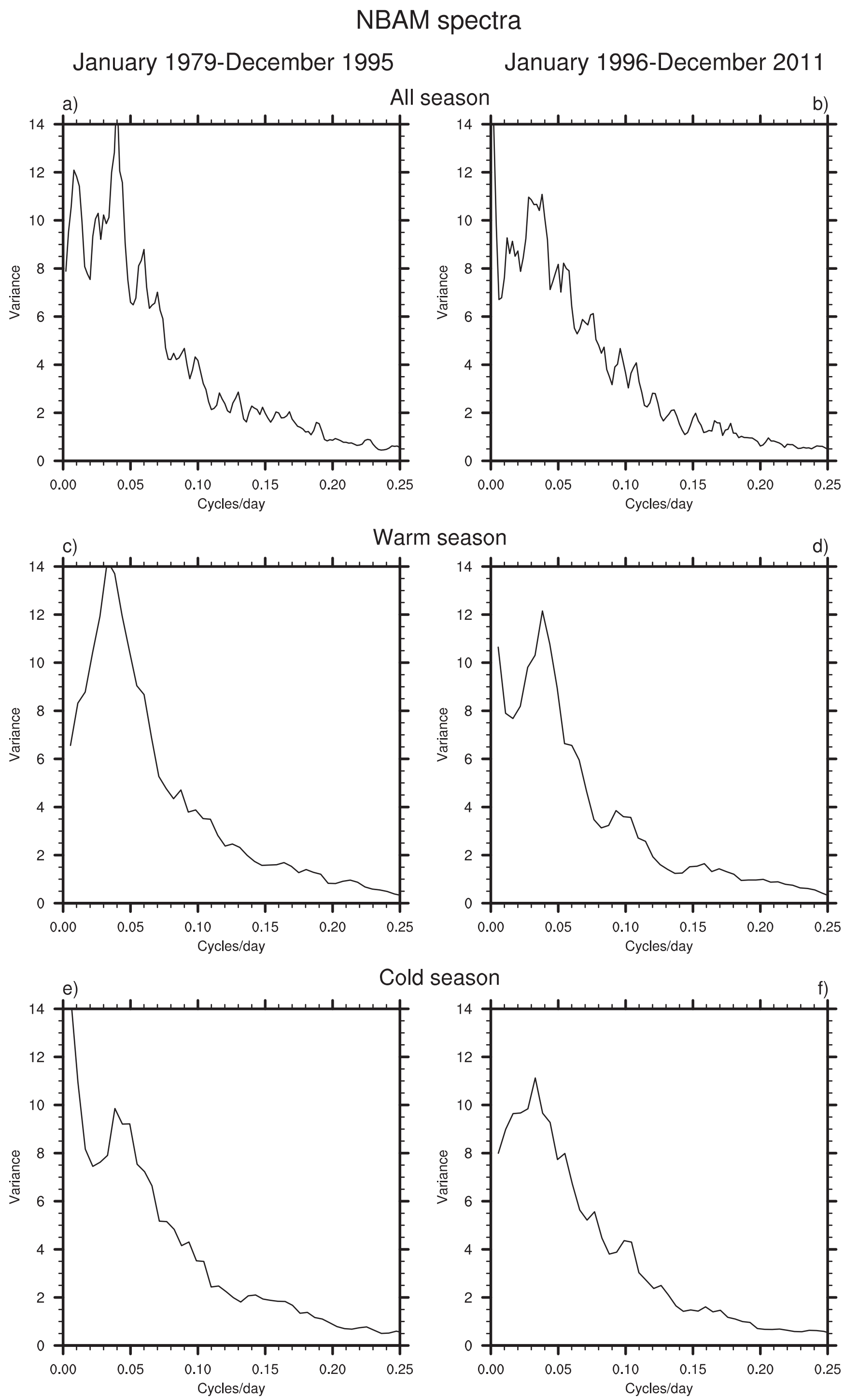


FIG. A1. (top) As in Fig. 12 and (middle),(bottom) as in Fig. 13, except showing spectra of the NBAM for (a),(c),(e) the first half of the data record and (b),(d),(f) the second half.

wind (Wettstein and Wallace 2010), 2) the root-mean-square (rms) 2.5–6-day bandpass-filtered midtropospheric geopotential height field (Lau 1988), and 3) the 8-day high-pass-filtered 850-hPa meridional eddy heat flux (Nakamura et al. 2002). A key distinction between the NBAM and the modes of pulsing storm-track activity identified in previous studies lies in their zonal scales. Wettstein and Wallace (2010) note that the linkages between variability in the North Pacific and North Atlantic storm tracks are very weak, and thus focus primarily on patterns of storm-track activity within the two ocean basins. The results shown here suggest that the linkages between eddy kinetic energy in the Pacific and Atlantic storm-track regions are statistically significant. In a companion study (E. P. Gerber and D. W. J. Thompson 2014, unpublished manuscript), we examine to what extent the weak but significant correlations between eddy kinetic energy over the two storm-track regions contribute to the hemispheric-scale structure of the NBAM.

A notable distinction between the analyses used to identify baroclinic annular variability in the Southern and Northern Hemispheres lies in the filtering of the wave fluxes. The baroclinic annular modes are consistent with two-way feedbacks between the baroclinicity and the wave fluxes of heat by synoptic-scale waves (Thompson and Barnes 2014). In the SH, the total variance in the eddy kinetic energy is dominated by waves on synoptic scales, and thus the SBAM emerges from PC analysis of the full eddy kinetic energy field. However, in the NH the total variance in the eddy kinetic energy field includes a substantial contribution from the planetary-scale waves. For this reason, the NBAM emerges most clearly from PC analysis of the eddy kinetic energy field after the variance due to planetary-scale waves has been filtered from the data.

As is the case in the SH, the two primary NH annular modes play very different roles in cycling energy through the NH circulation. The baroclinic annular mode (the NBAM) is linked primarily to variability in 1) the conversions between available zonal-mean and eddy potential energy and 2) the eddy kinetic energy (Fig. 5, right). The barotropic annular mode (the NAM) is linked primarily to variability in 1) the conversions between eddy and zonal-mean kinetic energy and 2) the zonal-mean kinetic energy (Fig. 5, left). The NBAM exhibits statistically significant periodicity on time scales of ~20–25 days that is most clear during the summer season. But the spectral peak in the NBAM index is generally less robust than that associated with the SBAM. We are currently investigating the climate impacts of the NBAM and the implications of its periodic behavior for NH climate variability.

*Acknowledgments.* We thank John M. Wallace and two anonymous reviewers for their helpful comments on the manuscript. DWJT is funded by the NSF Climate Dynamics program. YL is funded by *CloudSat* via NASA JPL and the NSF Climate Dynamics Program.

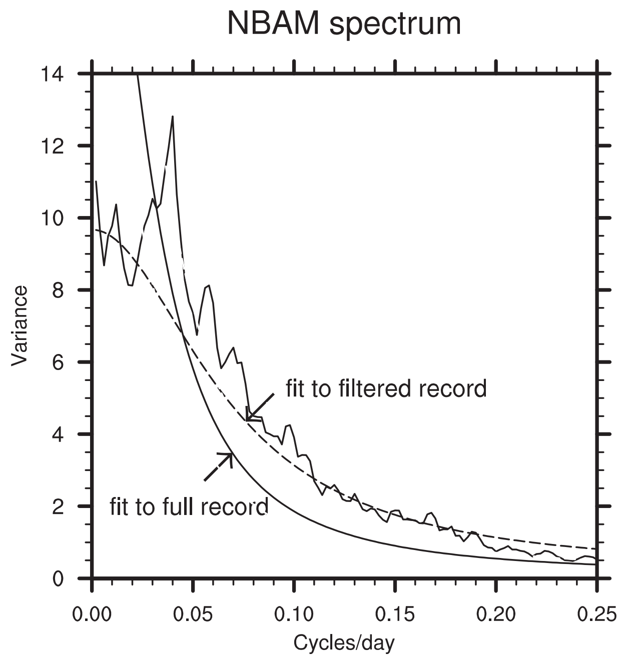


FIG. A2. The power spectra of the NBAM index (reproduced from Fig. 12) superposed on red-noise fits based on the autocorrelation of the unfiltered NBAM index (solid) and the 20-day high-pass-filtered NBAM index (dashed).

# APPENDIX

## Power Spectra of the NBAM Index

### *a. Spectra for subsets of the data*

Figure A1 shows spectra of the NBAM for all calendar days (top) and the NH warm and cold seasons (middle and bottom, respectively) calculated for the first and second halves of the data record. The left column shows results for 1979–95; the right column results for 1996–2011.

### *b. Red-noise fits to the power spectra*

The broad spectral peak at low frequencies in the NBAM index contributes to its lag-1 autocorrelation. As such, the red-noise fit based on the lag-1 autocorrelation of the NBAM index is distorted toward the low-frequency end of the spectrum. For example, Fig. A2 shows the spectrum of the NBAM index reproduced from Fig. 12. The red-noise fit indicated by the solid line is based on the lag-1 autocorrelation of the unfiltered NBAM index. It clearly overestimates the amount of power in the red-noise fit at low frequencies, but underestimates the amount of power in the fit at high frequencies (the area under the fit is equal to the area under the NBAM spectrum).

The component of the NBAM index that can be modeled as red noise is best estimated from the lag-1 autocorrelation of the NBAM index after it has been filtered to remove the broad spectral peak at low frequencies. The dashed line in Fig. A2 shows the red-noise fit based on the lag-1 autocorrelation of the 20-day high-pass-filtered NBAM index. The resulting red-noise fit evidently provides a much more realistic ‘‘background’’ spectrum against which the peak at low frequencies can be tested. The red-noise fit in Fig. 12 is based on the lag-1 autocorrelation of 20-day high-pass-filtered data. The red-noise fits in Fig. 13 are based on the lag-1 autocorrelations of 30-day high-pass-filtered data.

## REFERENCES


Ambaum, M. H. P., and L. Novak, 2014: A nonlinear oscillator describing storm track variability. *Quart. J. Roy. Meteor. Soc.,* **140,** 2680–2684, doi:10.1002/qj.2352.

Bretherton, C. S., M. Widmann, V. P. Dymnikov, J. M. Wallace, and I. Blade, 1999: The effective number of spatial degrees of freedom of a time-varying field. *J. Climate,* **12,** 1990–2009, doi:10.1175/1520-0442(1999)012<1990:TENOSD>2.0.CO;2.

Chang, E. K. M., 2004: Are the Northern Hemisphere winter storm tracks significantly correlated? *J. Climate,* **17,** 4230–4244, doi:10.1175/JCLI3195.1.

——, and D. B. Yu, 1999: Characteristics of wave packets in the upper troposphere. Part I: Northern Hemisphere winter. *J. Atmos. Sci.,* **56,** 1708–1728, doi:10.1175/1520-0469(1999)056<1708:COWPIT>2.0.CO;2.

——, and Y. Fu, 2002: Interdecadal variations in Northern Hemisphere winter storm track intensity. *J. Climate,* **15,** 642–658, doi:10.1175/1520-0442(2002)015<0642:IVINHW>2.0.CO;2.

Dee, D. P., and Coauthors, 2011: The ERA-Interim reanalysis: Configuration and performance of the data assimilation system. *Quart. J. Roy. Meteor. Soc.,* **137,** 553–597, doi:10.1002/qj.828.

DeWeaver, E., and S. Nigam, 2000: Do stationary waves drive the zonal-mean jet anomalies of the northern winter? *J. Climate,* **13,** 2160–2176, doi:10.1175/1520-0442(2000)013<2160:DSWDTZ>2.0.CO;2.

Feldstein, S. B., 2003: The dynamics of NAO teleconnection pattern growth and decay. *Quart. J. Roy. Meteor. Soc.,* **129,** 901–924, doi:10.1256/qj.02.76.

Gerber, E. P., and G. K. Vallis, 2005: A stochastic model for the spatial structure of annular patterns of variability and the North Atlantic Oscillation. *J. Climate,* **18,** 2102–2118, doi:10.1175/JCLI3337.1.

Hartmann, D. L., and F. Lo, 1998: Wave-driven zonal flow vacillation in the Southern Hemisphere. *J. Atmos. Sci.,* **55,** 1303–1315, doi:10.1175/1520-0469(1998)055<1303:WDZFVI>2.0.CO;2.

Hurrell, J. W., 1995: Decadal trends in the North Atlantic Oscillation: Regional temperatures and precipitation. *Science,* **269,** 676–679, doi:10.1126/science.269.5224.676.

Kidson, J. W., 1988: Interannual variations in the Southern Hemisphere circulation. *J. Climate,* **1,** 1177–1198, doi:10.1175/1520-0442(1988)001<1177:IVITSH>2.0.CO;2.

Lau, N.-C., 1988: Variability of the observed midlatitude storm tracks in relation to low-frequency changes in the circulation pattern. *J. Atmos. Sci.,* **45,** 2718–2743, doi:10.1175/1520-0469(1988)045<2718:VOTOMS>2.0.CO;2.

Li, Y., and N.-C. Lau, 2012: Contributions of downstream eddy development to the teleconnection between ENSO and the atmospheric circulation over the North Atlantic. *J. Climate,* **25,** 4993–5010, doi:10.1175/JCLI-D-11-00377.1.

Limpasuvan, V., and D. L. Hartmann, 2000: Wave-maintained annular modes of climate variability. *J. Climate,* **13,** 4414–4429, doi:10.1175/1520-0442(2000)013<4414:WMAMOC>2.0.CO;2.

Lorenz, D. J., and D. L. Hartmann, 2001: Eddy–zonal flow feedback in the Southern Hemisphere. *J. Atmos. Sci.,* **58,** 3312–3327, doi:10.1175/1520-0469(2001)058<3312:EZFFIT>2.0.CO;2.

——, and ——, 2003: Eddy–zonal flow feedback in the Northern Hemisphere winter. *J. Climate,* **16,** 1212–1227, doi:10.1175/1520-0442(2003)16<1212:EFFITN>2.0.CO;2.

Nakamura, H., T. Izumi, and T. Sampe, 2002: Interannual and decadal modulations recently observed in the Pacific storm track activity and East Asian winter monsoon. *J. Climate,* **15,** 1855–1874, doi:10.1175/1520-0442(2002)015<1855:IADMRO>2.0.CO;2.

North, G. R., T. L. Bell, R. F. Cahalan, and F. J. Moeng, 1982: Sampling errors in the estimation of empirical orthogonal functions. *Mon. Wea. Rev.,* **110,** 699–706, doi:10.1175/1520-0493(1982)110<0699:SEITEO>2.0.CO;2.

Quadrelli, R., and J. M. Wallace, 2004: A simplified linear framework for interpreting patterns of Northern Hemisphere wintertime climate variability. *J. Climate,* **17,** 3728–3744, doi:10.1175/1520-0442(2004)017<3728:ASLFFI>2.0.CO;2.

Simmons, A. J., and B. J. Hoskins, 1978: The life cycles of some nonlinear baroclinic waves. *J. Atmos. Sci.,* **35,** 414–432, doi:10.1175/1520-0469(1978)035<0414:TLCOSN>2.0.CO;2.

Thompson, D. W. J., and J. M. Wallace, 2000: Annular modes in the extratropical circulation. Part I: Month-to-month variability. *J. Climate,* **13,** 1000–1016, doi:10.1175/1520-0442(2000)013<1000:AMITEC>2.0.CO;2.

——, and E. A. Barnes, 2014: Periodic variability in the large-scale Southern Hemisphere atmospheric circulation. *Science,* **343,** 641–645, doi:10.1126/science.1247660.

——, and J. D. Woodworth, 2014: Barotropic and baroclinic annular variability in the Southern Hemisphere. *J. Atmos. Sci.,* **71,** 1480–1493, doi:10.1175/JAS-D-13-0185.1.

Wallace, J. M., 2000: North Atlantic Oscillation/annular mode: Two paradigms—One phenomenon. *Quart. J. Roy. Meteor. Soc.,* **126,** 791–805, doi:10.1002/qj.49712656402.

——, and D. S. Gutzler, 1981: Teleconnections in the geopotential height field during the Northern Hemisphere winter. *Mon. Wea. Rev.,* **109,** 784–812, doi:10.1175/1520-0493(1981)109<0784:TITGHF>2.0.CO;2.

Wettstein, J. J., and J. M. Wallace, 2010: Observed patterns of month-to-month storm track variability and their relationship to the background flow. *J. Atmos. Sci.,* **67,** 1420–1437, doi:10.1175/2009JAS3194.1.